Colloid Polym Sci (2008) 286:1029–1037
DOI 10.1007/s00396-008-1866-2

ORIGINAL CONTRIBUTION

Generation and electrical contacting of gold quantum dots

G. Schmid · T. Reuter · U. Simon · M. Noyong · K. Blech · V. Santhanam · D. Jäger · H. Slomka · H. Lüth · M. I. Lepsa

Received: 12 February 2008 / Accepted: 5 March 2008 / Published online: 20 April 2008

Abstract We report on first tries in generating a system of 20-nm-wide parallel bars as templates for conductive gold wires, decorated with $Au_{55}(PPh_3)_{12}Cl_6$ clusters. The electrical characterization of these quasi one-dimensional arrangements shows pronounced nonlinearity, reflecting charging effects on the small clusters. Furthermore, very first results on the generation of 2.5-nm bars are also reported.

Keywords Hybrid materials · Molecular electronics · Quantum dots · Self-assembled monolayers · Nanostructures · Nanowires · Electrodes · Nanoparticles · Conductivity

G. Schmid · T. Reuter
Universität Duisburg-Essen,
Universitätsstrasse 1,
45127 Essen, Germany

U. Simon · M. Noyong · K. Blech · V. Santhanam
RWTH Aachen University, Jülich-Aachen Research Alliance (JARA),
Landoltweg 1,
52074 Aachen, Germany

D. Jäger · H. Slomka
Universität Duisburg-Essen,
Lotharstr. 55 (ZHO),
47057 Duisburg, Germany

H. Lüth · M. I. Lepsa
Forschungszentrum Jülich (IBN-1),
Jülich-Aachen Research Alliance (JARA),
52428 Jülich, Germany

U. Simon (✉)
Institute of Inorganic Chemistry, RWTH Aachen University,
52056 Aachen, Germany
e-mail: ulrich.simon@ac.rwth-aachen.de

Introduction

Quantum dots are generally considered as possible building blocks in future nanoelectronic devices due to their specific properties. Metal nanoparticles exhibit size-dependent properties of various kinds. The well-known plasmon resonance of some metals in the visible range appears, if light interacts with the confined electron gas of a particle, small enough to enable a collective electron oscillation. Size-dependent magnetic phenomena have become known as well as deviations of the electric conductivity, compared with bulk metals. A very special quantum dot has been found in $Au_{55}(PPh_3)_{12}Cl_6$ with its 1.4-nm core [1, 2]. Its quantized nature becomes visible already at room temperature and not only at low temperatures as in the case for larger particles. Just slightly enlarged metal nanoparticles behave already bulk-like at room temperature, which has been shown for 1.8-nm Pt clusters [3]. Numerous investigations on individual Au_{55} clusters proved their unique electronic nature, especially the capability to act as a single-electron switch at room temperature, indicated by a well-defined Coulomb blockade in the current–voltage characteristic [4]. At 7 K, the cluster even exhibits discrete electronic energy levels, justifying the expression "artificial atom" [5, 6].

Of course, our knowledge on the single electron storage behavior of individual ligand-protected Au_{55} clusters provoked questions concerning possible future applications. Numerous investigations of three- and two-dimensional cluster arrangements resulted in informative facts on the electronic interactions between these quantum dots, separated by different ligand shells [7–16]. However, the ultimate challenge is the processing of single electron switches and transistor arrays and their individual addressing from the outside. The difficulties are quite obvious: Besides the development of a two-dimensional cluster

arrangement, electronically conductive leads of appropriate dimension have to be generated for the interconnection as well as electrically addressing the quantum dots.

Self-assembly of ligand-protected Au_{55} clusters has been observed [17, 18], and low-dimensionally controlled assembly has been realized by atomic force microscopy (AFM) techniques [19]. However, though perfectly developed architectures resulted, they were not suited for the purposes under discussion. Therefore, we were looking for another technique to reach this goal, not yet under ultimate conditions but in a first approach, to reach at least the proof of the principle. A promising technique is molecular beam epitaxy for the generation of stacks of several bars. Those bars have controllable widths and can be used as templates for metal nanowires with diameters down to 10 nm [20]. The final goal is to elaborate a cross bar system of 2.5-nm gold nanowires, containing single Au_{55} clusters at each of the crossing points. This paper reports on first tries in generating a system of 20-nm parallel conductive gold wires, decorated with $Au_{55}(PPh_3)_{12}Cl_6$ clusters and on the electrical characterization of these quasi one-dimensional arrangements. The very first results on the generation of 2.5-nm bars are also reported.

Results and discussion

Generation of custer-decorated 20-nm gold nanowires

To generate groups of parallel 20-nm-wide gold wires, we used a technique, which is based on the fabrication of a multilayer system consisting of epitaxially grown alternating GaAs and AlAs layers. Recently, a similar process has been used to generate a stamp system for a successive nanoimprint procedure [21]. Figure 1 elucidates the process.

After growing the superlattice of GaAs and AlAs on semi-insulating (SI) GaAs wafers, an oxidation step using 30% H_2O_2 transformed the surface layer into Ga_2O_3 and Al_2O_3. Treatments of 60 s turned out to give well-defined structures. In a second step, we used citric acid to dissolve the Ga_2O_3 from the surface, leaving 20-nm Al_2O_3 bars. Finally, another oxidation step followed to transfer the underlying arsenides into oxides to have a nonconducting substrate for the following electrical measurements. The resulting structures were investigated by means of AFM and scanning electron microscopy (SEM). Figure 2a shows an AFM image of an array of 20-nm Al_2O_3 bars, and in Fig. 2b and c, corresponding SEM images are shown.

Figure 2b demonstrates that the bars are running perfectly parallel, whereas the distances between them are varying to some extent. From Fig. 2c, it can be seen that some of the bars are occasionally bent, probably due to capillary forces during the wet etching process.

The next step consisted of the covering of the oxide bars with gold, using an electron beam evaporation device. The gold coating was performed under an angle of 45° to achieve a shadow mask deposition to prevent coating of the interspaces. The thickness of the gold layer was 15 nm. Figure 3 shows a sketch of this process.

The proof of the successful gold wire generation was performed by SEM and energy-dispersive X-ray spectros-

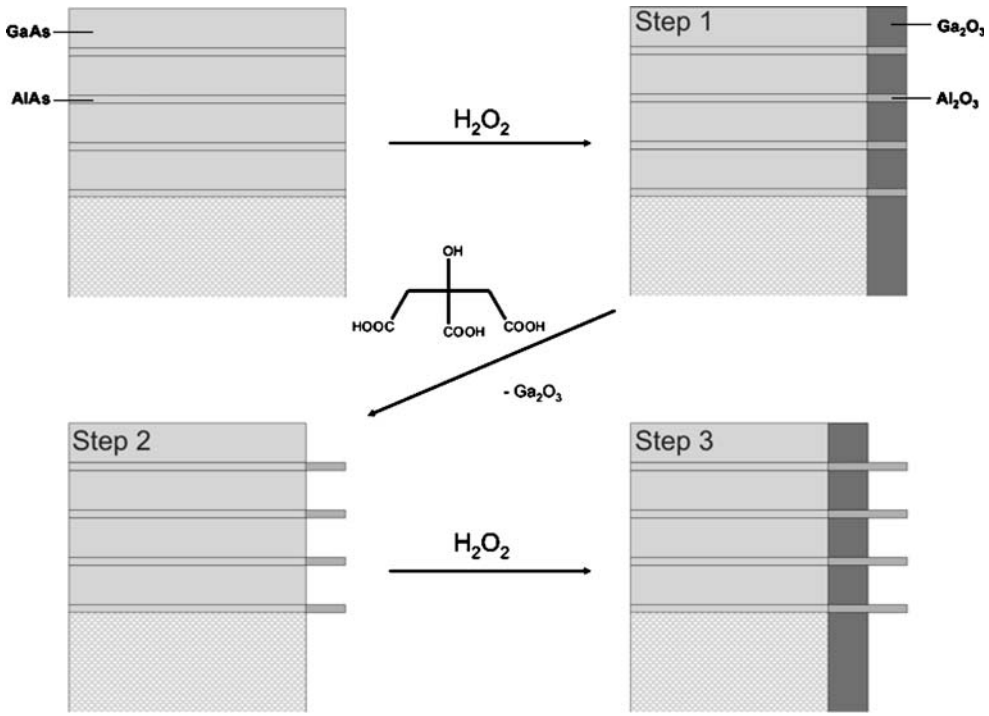

Fig. 1 Sketch of the three steps to define Al_2O_3 bars from a GaAs/AlAs superlattice. *Step 1*: Oxidation of the surface layer by H_2O_2. *Step 2*: Chemical etching by citric acid and *step 3*: repeated oxidation by H_2O_2

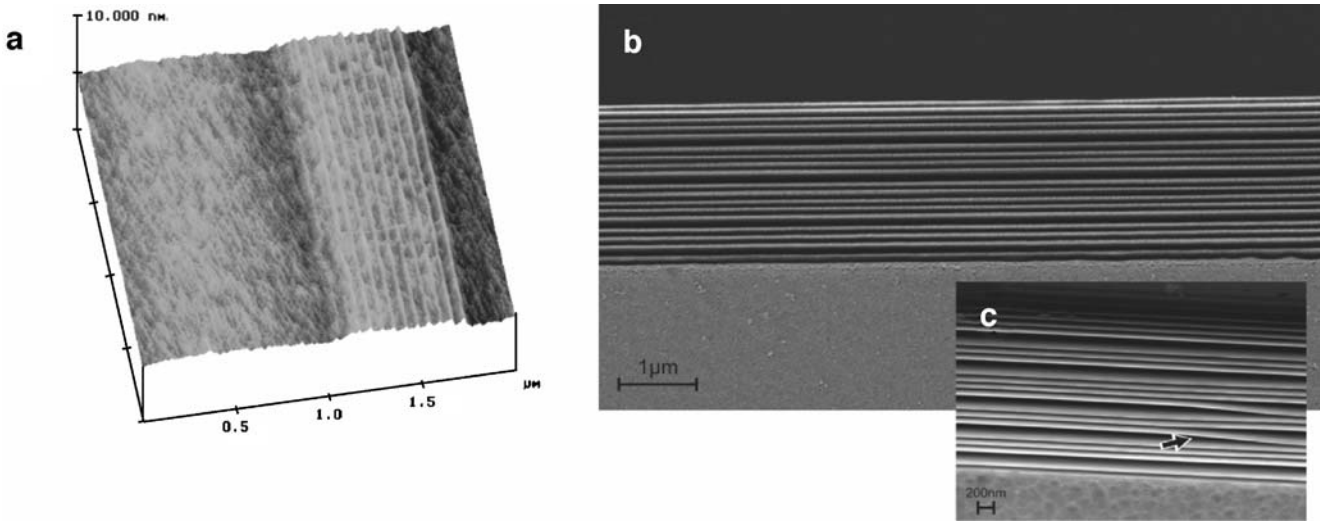

Fig. 2 **a** AFM image of a 20-nm-etched structure. **b** SEM image showing parallel 20 nm Al_2O_3 bars. **c** SEM image of an occasionally observed bent bar (*arrow*)

copy (EDX) analyses showing qualitatively the presence of Au. A quantitative analysis was not possible due to the topography of the structure.

For the deposition of $Au_{55}(PPh_3)_{12}Cl_6$ clusters on the gold wires, we followed a procedure that has been before successfully applied to generate cluster monolayers on gold surfaces [22]. From these studies, it is known that the thiol stands almost upright on an Au surface with its free thiol group remaining accessible for the Au nanoparticle immobilization. The samples with gold wires were dipped into *n*-heptane solutions of 1,4-benzenedithiol for 15 h. After washing with *n*-heptane and drying, the fixation of the clusters was performed by immersing the sample in a dichloromethane cluster solution for 3 h. Washing with CH_2Cl_2 to remove excessive clusters and subsequent drying resulted in the structures used for the electrical measurements. The covalent binding of the clusters is the result of the partial substitution of PPh_3 ligands by the free thiol groups of 1,4-benzenedithiol. Figure 4 shows a sketch of an as-prepared sample.

The direct proof of the existence of cluster-covered gold wires is not possible, since the resolution of SEM is not high enough, and EDX analyses indicate the existence of gold in any case due to the presence of the gold wires. However, indirect evidence can be deduced from AFM measurements by partially removing of the bound cluster layer by scratching, obtaining height difference of about 3 nm (see Fig. 5) [23, 24]. Although this height is slightly larger than it is expected from a monolayer of a single Au_{55}

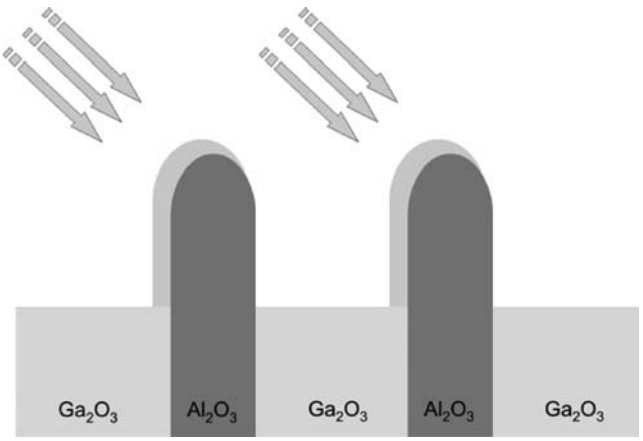

Fig. 3 Scheme of the shadow mask deposition of gold on Al_2O_3 bars

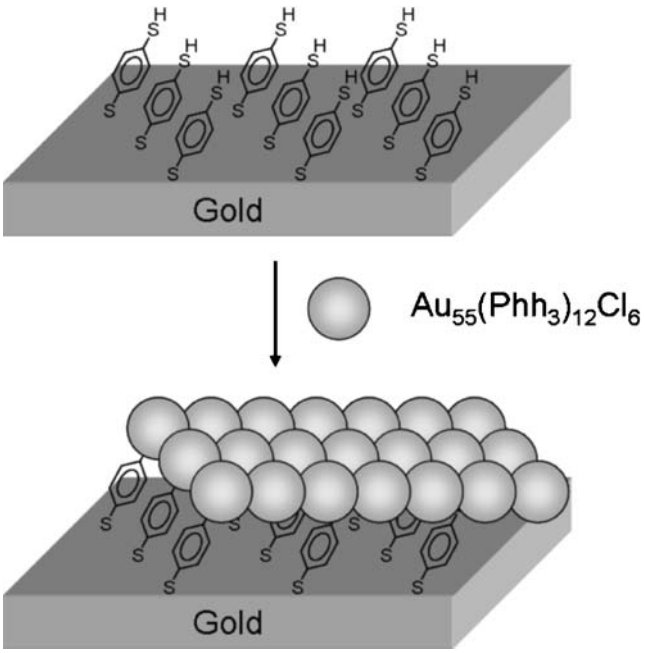

Fig. 4 Self-assembled 1,4-benzenedithiol molecules chemisorbing $Au_{55}(PPh_3)_{12}Cl_6$ clusters

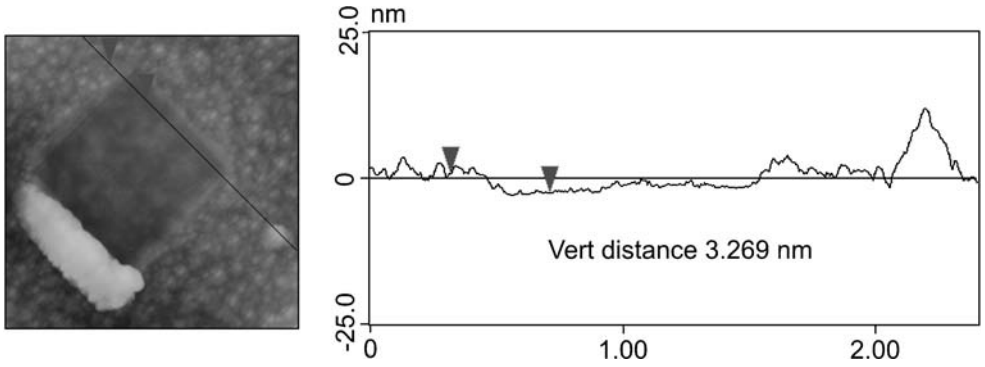

Fig. 5 AFM image and cross-section of partially removed layer of chemisorbed $Au_{55}(PPh_3)_{12}Cl_6$ clusters on gold

cluster on 1,4-benzenedithiol, we conclude that clusters are immobilized and densely packed on the gold wires. This encouraged us to perform further electrical measurements.

Electrical measurements

Electrical measurements (DC) were performed on an in situ probing setup in a scanning electron microscope [25, 26]. Noble metal-covered AFM tips with tip curvatures of down to 45 nm were used for local electrical addressing. Horizontal and vertical movement of these tips was realized by two nanorobotic systems with piezo-driven motors, which allow a precise positioning in a subnanometer length scale [27]. Reference measurements on a freshly cleaned Pt wire as well as short circuiting the tips themselves showed $I(U)$ curves with an ohmic behavior and a contact resistance of about 8 Ω [25, 26].

For probing the electrical conductance of the applied gold layer, the first set of experiments was performed on 20-nm Al_2O_3 bars covered with gold. The electrical contact was achieved by moving the tips downward onto the bar structure. After the first visible lateral movement of each tip (reflecting a mechanical contact), the electrical measurements were started. Figure 6 shows an SEM image and the $I(U)$ curves of a substrate with 20-nm-wide lines covered with 100 nm (Fig. 6a and b) and a 15 nm (Fig. 6c and d) thick gold layer, respectively. These as well as all further measurements were performed with a current limitation at 50 nA on structures without clusters and 25 nA on structures with clusters to avoid current-induced thermal decomposition of the layers. Although the $I(U)$ measurements on the 100-nm-thick layers were found to be more stable than those on the 15-nm layers, in both cases, ohmic behavior was observed. If the mechanical force to the tips was increased, a deformation or even a destruction of the Au wires occurred (see inset in Fig. 6c), resulting in unstable electrical contacts. Furthermore, the measurements were complicated by the thermal drift of the sample stage during the measurements.

The resistances determined from the $I(U)$ curves of the samples with 100- and 15-nm gold layers were 2.5 MΩ, from which a resistivity of 4.4×10^{-3} and $1.9\cdot10^{-3}$ Ωm, respectively, can be derived. For this estimation, we regarded the gold layers as wires with 100- and 15-nm diameter, respectively, and a circular contact area corresponding to the tip diameter, i.e., 45 nm. In this study, we found a slightly higher value for the 100-nm-thick structure, which may be attributed to a higher surface roughness. The contact resistance between the tips and a metallic substrate is typically in the range of a few ohms, so that it can be neglected. In general, the resistivities found are much higher than the bulk value for metallic gold, which may predominantly be caused by surface and interparticle-scattering effects.

The next set of experiments was then performed on gold structures with immobilized clusters. The $I(U)$ curves were recorded in different distances of the tips (Fig. 7).

All $I(U)$ curves recorded show a significantly higher resistivity for the structures with clusters. Both sets of curves reflect a pronounced nonlinearity. At the same time, the resistance increases with increasing tip-to-tip distance.

To compare the resistances of the structures without and with clusters, we determined the resistances for the low- (±0.25 V) and high-field (>0.5 V) data presented in Fig. 7.

Since the clusters are too small to be imaged by SEM on the underlying gold substrate, the electrical measurements serve as an indirect prove for the presence of the clusters. Thus, we attribute the increase in resistance between samples without and with the cluster layer to the tunneling contacts introduced by the clusters and their immobilization layer, while the increasing nonlinearity together with the strong increase in resistance with increasing tip-to-tip distances reflects granularity/grain boundaries in the gold layer. The granularity is visible in Fig. 6a, and it is probably the reason for the higher resistivity of the thicker 100-nm gold layer compared to the 15-nm layer. Furthermore, the granularity may also affect the contact area. The contribution of the cluster layer to the total resistance can be derived from the resistance in the low- and high-field areas (Fig. 8).

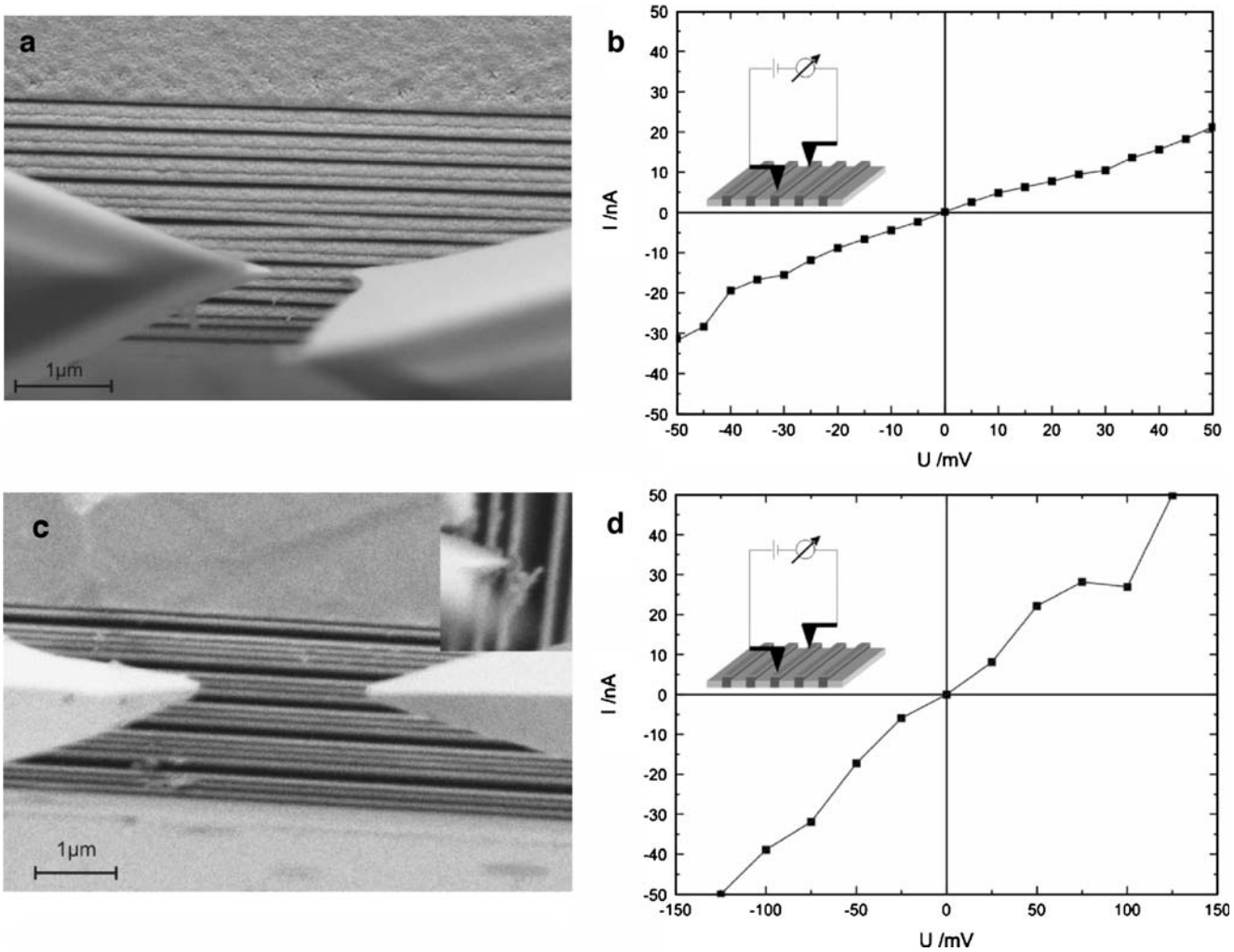

Fig. 6 Contacting tips and typical sample with 20-nm-wide Al_2O_3 bars and **a** 100- and **c** 15-nm-thick gold layers. **b**, **d** Corresponding *I* (*U*) curves of single bars for tip-to-tip-distances of 0.9 and 2.1 μm, respectively. The *inset* in **c** shows a destroyed gold layer after applying a too high force. *I*(*U*) curves achieved represent the best conductivity during contacting the samples with a set of measuring tips. Cleaning using oxygen plasma gave no further increase in conductivity

Comparing samples without and with clusters, we found that the additional resistance can be calculated to be about 26 MΩ (for 2 μm tip-to-tip distance) at low fields and 8 MΩ at high fields, respectively.

To estimate the resistance of the individual clusters, we need to estimate how many clusters are involved in the charge transfer process at the contact area between tips and Au wires. With a tip diameter of about 45 nm, each tip could cover an area of up to 1,800 nm^2 on a single bar structure. In an ideally close packed layer, up to 270 clusters can be placed on this area. When we assume this amount of clusters under each tip and a resistance of the cluster layer of 26 MΩ, the resistance of a single cluster is about 3.5 GΩ. For comparison at low fields in scanning tunneling spectroscopy (STS) measurements (below the Coulomb threshold) of isolated single clusters on a thiol-covered gold substrate, a resistance of 2.6 GΩ was measured, which is in remarkable agreement with our result [28].

A second indication for the presence of the clusters on the gold wires is the appearance of the nonlinearity already at small tip-to-tip distance. While at larger distances, the *I* (*U*) is nonlinear in all cases, and the measurement at small distances without clusters exhibit almost metallic behavior. The addition of the clusters introduces the nonlinearity, reflecting the charging effects of the clusters as it is observed in one- and two-dimensional nanoparticle arrays [29]. STS measurements on Au_{55} clusters showed even at room temperature a discrete Coulomb blockade (zero conductance around U=0 V) [4, 28, 30]. This can also be seen in STS measurements on monolayers of silver nanoparticles, which were reported by Taleb et al. [31]. In such layers, a nonlinear *I*(*U*) curve is observed, but a distinctive Coulomb blockade is absent. This effect was explained by a

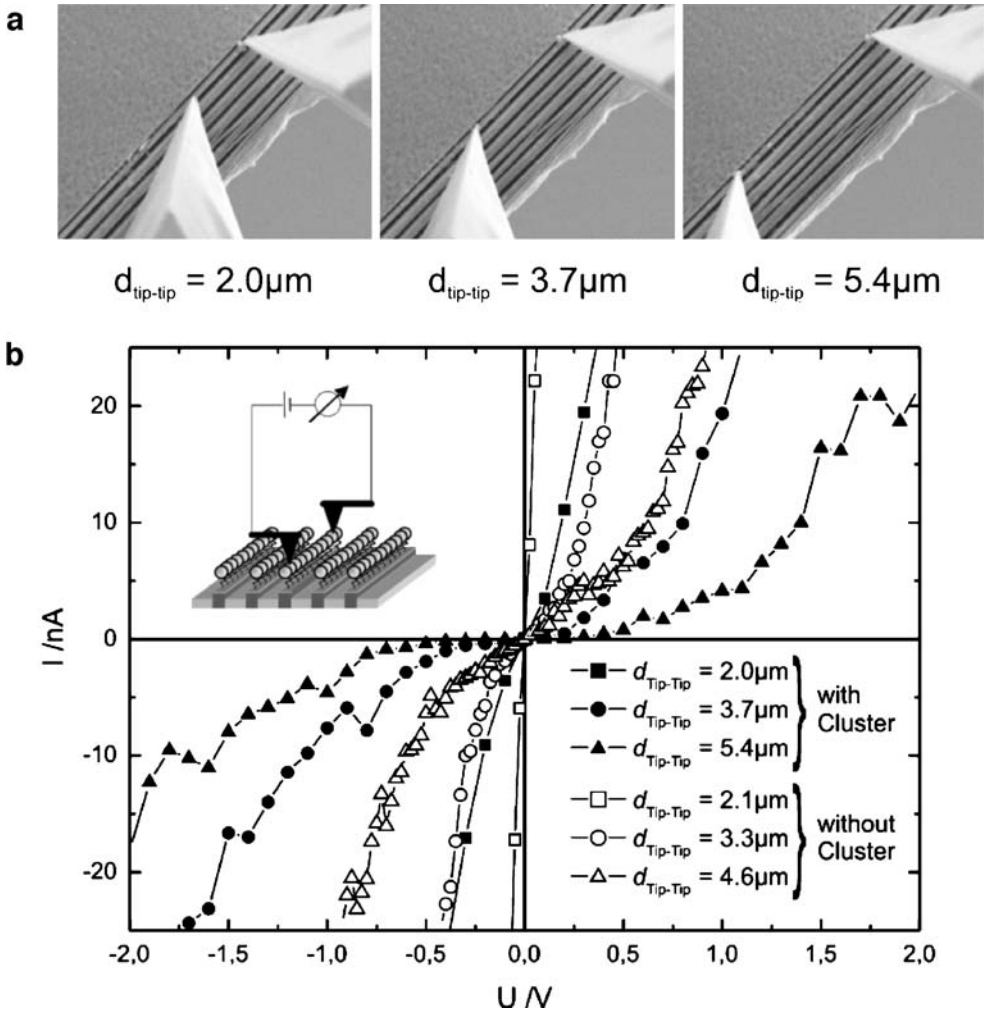

Fig. 7 **a** SEM images of different tip–tip distances on a sample with gold clusters with corresponding $I(U)$ curves (**b**). For comparison, the $I(U)$ curves on bare gold wires are added

lateral electron transport parallel to the surface through the cluster layer. Thus, the effective capacitance between the particle and substrate is increased. Ohgi et al. reported on similar STS measurements on layers of 5-nm gold nanoparticles [32]. They described that the Coulomb blockade gap size decreases with increasing coverage of the nanoparticle on the surface. This effect was also explained by interparticle contacts, which increases the effective capac-

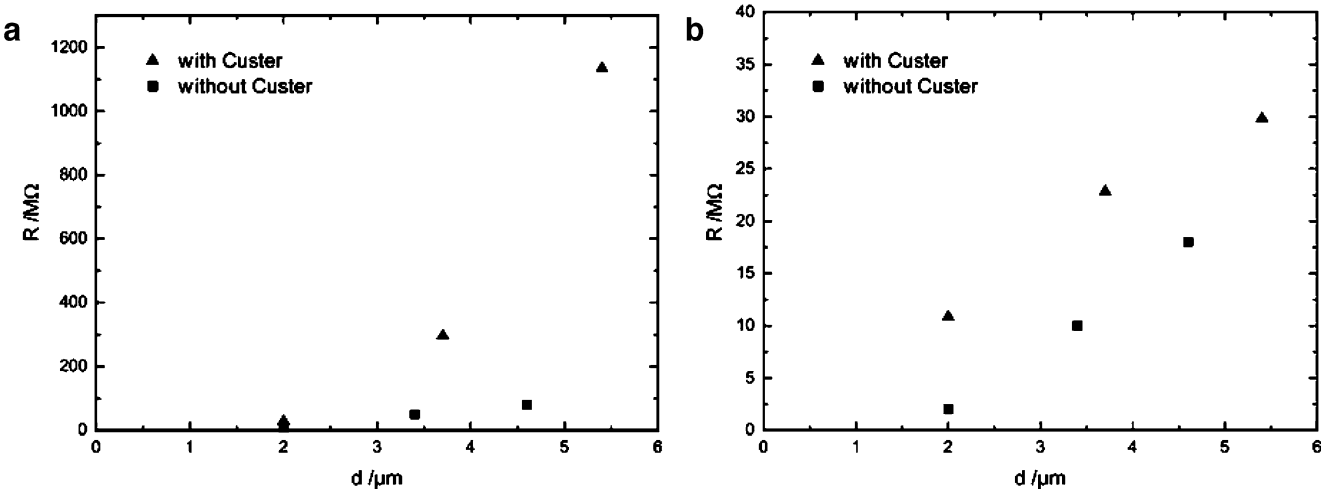

Fig. 8 Resistances derived from low- (**a**) and high-field (**b**) data (taken from Fig. 7)

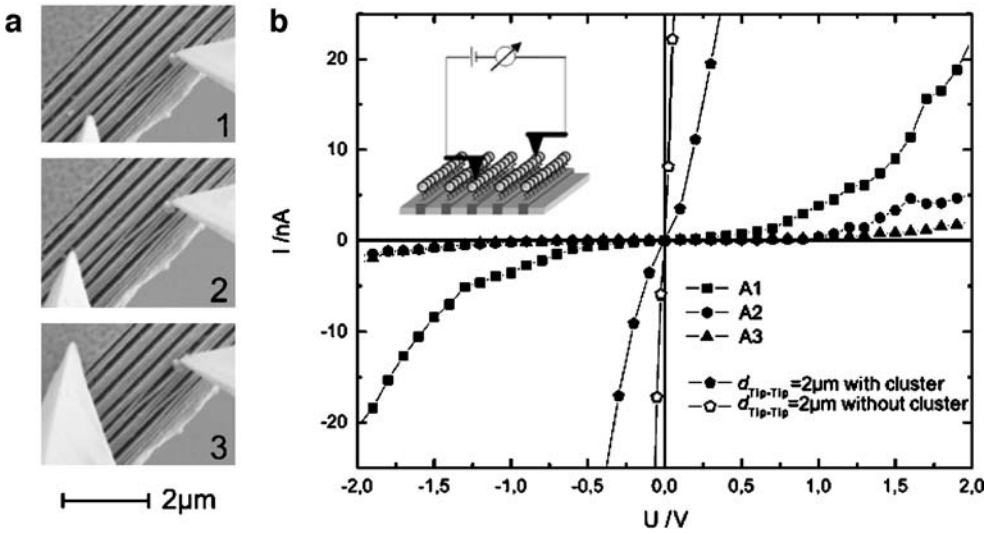

Fig. 9 **a** SEM images and **b** electrical measurements with different tip positions without direct connection between the tips: *A1*, two neighbored bar structures with transversal single bar, *A2* left-handed tip placed on bars without visible connection to right handed tip, *A3* left-handed tip placed on the gold-covered, unstructured area. For comparison, *I*(*U*) curves on bare gold wires and gold wires with attached clusters (tip-to-tip distance, 2 μm) are added

itance, and hence the zero voltage area gets smaller. Thus, the absence of a discrete Coulomb blockade in our experiments can be attributed to the fact that our contact tips address several clusters in parallel.

To evaluate how much current can be observed between two neighboring Au wires, which might represent a parasitic effect for the individual lines, we measured the current between tips, which were placed on different bars. Figure 9 shows several measurements, in which one tip (the left one in Fig. 9) was placed on a neighboring bar, on the next neighboring bar, or on the fully metalized area (edge of the supporting GaAs wafer). For these positions of the tips, the resistances are found to be 1.2, 33, and 18 GΩ. Thus, the resistances, which are three orders of magnitude higher than along the leads, as well as the rapid resistivity increase perpendicular to the leads, illustrate the low and therefore negligible parasitic current.

First approaches to 2.5-nm structures

Using a slight modified epitaxial growth and etching processes, we started to generate the ultimate small structures of 2.5 nm width for realizing the final goal, mentioned above. Whereas on 20-nm-wide gold wires, up to nine $Au_{55}(PPh_3)_{12}Cl_6$ clusters can be deposited in parallel, on 2.5-nm-wide bars, we should obtain strictly one-dimensional cluster arrangements, resulting in one single cluster between crossing bars. A surplus of clusters outside of the cross-point of gold wires would be without function and therefore irrelevant.

It must be stated that this approach will still take many independent developments of various techniques, necessary to fabricate a cross-bar system with individually contacted 2.5-nm gold wires. However, the first necessary step of this process namely, the generation of approximately 2.5-nm-wide

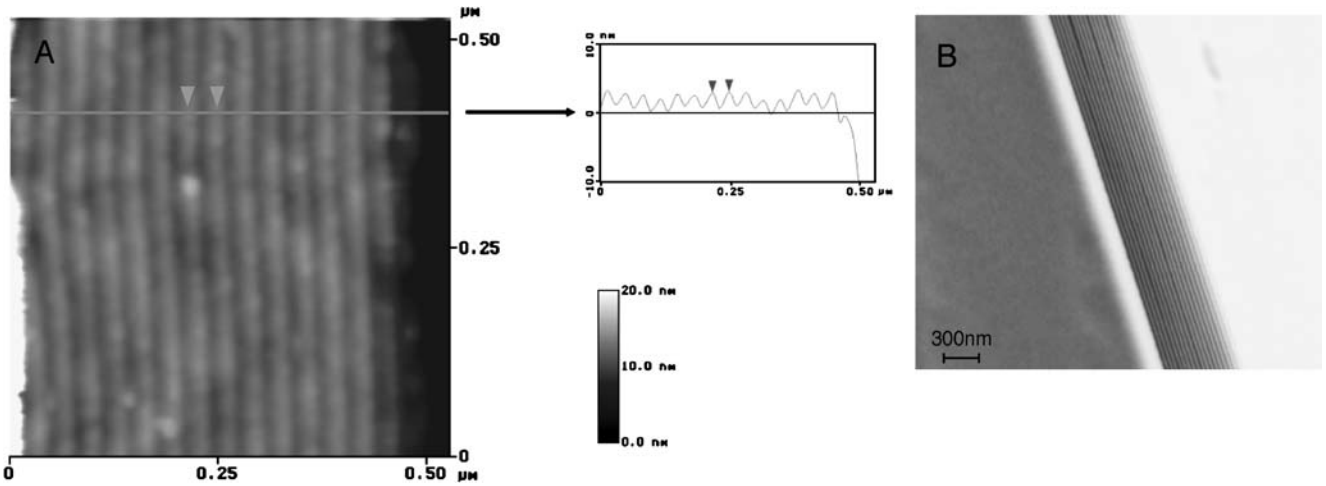

Fig. 10 **a** AFM image with cross-section and **b** SEM image of 2.5-nm-wide Al_2O_3 bars

Al_2O_3 bars from a corresponding superstructure, indeed succeeded. As can be seen from the AFM image in Fig. 10a, 2.5-nm lines after etching have been achieved.

The SEM image in Fig. 10b also demonstrates the successful generation of the 2.5-nm-wide Al_2O_3 bars, generated during the gradually elaborated technique. As well as on wider structures, a gold layer was deposited and functionalized with gold clusters.

Based on these results, it should be possible to reach the ultimate goal. However, it is obvious that the efforts will be enormous, reaching the limits of currently available measuring methods.

Conclusions

In this work, we have presented the preparation of Al_2O_3 bars with widths of 20 and 2.5 nm, respectively, starting from epitaxially grown GaAs/AlAs multilayers. The layer structures were used to fabricate parallel gold wires on which $Au_{55}(PPh_3)_{12}Cl_6$ clusters were immobilized. Electrical measurements on these cluster-coated gold wires exhibited the expected nonlinear $I(U)$ characteristics, which is attributed to the formation of tunneling barriers by the ligand shells in combination with charging effects of the small clusters. The derived resistance values were found to be in remarkable agreement with tunneling spectroscopy data. Thus, we have been able to show a first step toward a cross-bar device using a single-electron charging effect of individual chemically designed metal nanoparticles.

Experimental

Generation of cluster-decorated gold wires

Epitaxially generated 150-μm-thick multilayered GaAs/AlAs probes on SI-GaAS wafers, consisting of 20- or 2.5-nm AlAs layers, separated from each other by 100- and 35-nm GaAs layers, respectively, were cut into 5·2-mm^2 pieces. The 5-mm edges are used as the surfaces to be etched. The etching process was performed by using a mixture of citric acid (20 g in 20 mL deionized water) and 30% H_2O_2 in a 4:1 ratio. The samples were immersed in this solution for 60 s, followed by rinsing with deionized water for another 60 s. Thereafter, the samples were dipped into 30% H_2O_2 for 60 s, repeatedly rinsed with deionized water, and dried in a stream of dry nitrogen. For the final coverage of the Al_2O_3 bars with gold, a thermal evaporation device was used, operating at 1.5×10^{-6} mbar. The rate of evaporation was 0.1 nm Au per second. The vapor process was performed under an angle of 45°.

$Au_{55}(PPh_3)_{12}Cl_6$ was prepared as described elsewhere [1, 2].

For the deposition of the clusters on the gold wires, first *p*-1,4-benzenedithiol was bound to the gold surfaces using solutions of 1.5 mg of the dithiol in 3 mL *n*-heptane (2.5×10^{-3} mol L^{-1}). After 15 h, the samples were washed three times with *n*-heptane and dried by a stream of dry nitrogen. The as-prepared samples were then dipped into a 1×10^{-5}-mol L^{-1} (142 mg·mL^{-1}) dichloromethane solution of freshly Anatop-filtered $Au_{55}(PPh_3)_{12}Cl_6$ for 3 h, rinsed with CH_2Cl_2, and nitrogen dried.

Technical setup

A Riber 32 P molecular beam epitaxy system was used to generate the GaAs/AlAs multilayer probes.

Electrical addressing of the samples was performed in a scanning electron microscope (LEO Supra 35VP, Zeiss, Oberkochen, Germany) equipped with an in situ nanorobotics system (Klocke Nanotechnik, Aachen, Germany). The scanning electron microscope is equipped with a Gemini column (field emission electron gun) and secondary electron, in-lens, and backscattered secondary electron detectors for the high-vacuum (HV) mode and a variable-pressure (VP) secondary electron detector for the VP mode. All measurements were performed in the HV mode at pressures of about 10^{-5} mbar using an oil-free pumping system.

The in situ nanorobotics system is equipped with metal (Pt and Pt/Pd)-covered AFM tips (Klocke Nanotechnik, Aachen, Germany) with tip curvatures of down to 45 nm and a spring constant of 40 Nm^{-1}. Both end effectors are based each on three piezo-driven motors (*X*, *Y*, *Z* direction) and can position the contacting tips with subnanometer precision. Electrical measurements were recorded using a Parameter Analyzer 4156C (Agilent, Japan). Details of this experimental setup are described elsewhere [25, 26].

References

1. Schmid G, Boese R, Pfeil R, Bandermann F, Meyer S, Calis GHM, van der Velden JWA (1981) Chem Ber 114:3634
2. Schmid G (1990) Inorg Synth 7:214
3. Dubois JGA, Gerretsen JW, Shafranjuk SE, Boon EJG, Schmid G, van Kempen H (1996) Europhys Lett 33:279
4. Schmid G, Chi LF (1998) Adv Mater 10:515
5. Zhang H, Schmid G, Hartmann U (2003) Nanoletters 3:305
6. Zhang H, Hartmann U, Schmid G (2004) Appl Phys Lett 84:1543
7. Simon U, Schmid G, Schön G (1993) Angew Chem Int Ed Engl 32:250
8. Schmid G (2000) In: Schmid G (ed) Clusters and colloids: from theory to applications. VCH, Weinheim, p 178
9. Schön G, Simon U (1995) Colloid Polym Sci 273:101
10. Schön G, Simon U (1995) Colloid Polym Sci 273:202
11. Simon U (1998) Adv Mater 10:1487

12. Torma V, Reuter T, Vidoni O, Schumann M, Radehaus C, Schmid G (2001) ChemPhysChem 8/9:546
13. Torma V, Vidoni O, Simon U, Schmid G (2003) Eur J Inorg Chem 2003:1121
14. Schmid G, Simon U (2005) Chem Comm 2005:697
15. Reuter T, Neumeier S, Schmid G, Koplin E, Simon U (2005) Eur J Inorg Chem 2005:3670
16. Neumeier S, Reuter T, Schmid G (2005) Eur J Inorg Chem 2005:3679
17. Schmid G, Bäumle M, Beyer N (2000) Angew Chem Int Ed Engl 39:181
18. Schmid G, Beyer N (2000) Eur J Inorg Chem 2000:835
19. Liu S, Maoz R, Schmid G, Sagiv J (2002) Nanoletters 2:1055
20. Melosh NA, Boukai A, Diana F, Gerardot B, Badolato A, Petroff PM, Heath JR (2003) Science 300:112
21. Jung GY, Johnston-Halperin E, Wu W, Yu Z, Wang SY, Tong WM, Li Z, Green JE, Sheriff BA, Boukai A, Bunimovich Y, Heath JR, Williams RS (2006) Nanoletters 6:351
22. Vidoni O, Neumeier S, Bardou N, Pelouard JL, Schmid G (2003) J Cluster Sci 14:325
23. Santinacci L, Zhang Y, Schmuki P (2005) Surf Sci 597:11
24. Bhushan B, Koinkar VN (1994) Appl Phys Lett 64:1653
25. Noyong M, Blech K, Rosenberger A, Klocke V, Simon U (2007) Meas Sci Technol 18:N84
26. Blech K, Noyong M, Juillerat F, Hofmann H, Simon U (2008) J Nanosci Nanotech 8:461
27. Klocke Nanotechnik. Available at: www.nanomotor.de
28. Chi L, Hartig M, Drechsler T, Schwaack T, Seidel C, Fuchs H, Schmid G (1998) Appl Phys A 66:187
29. Elteto K, Lin X, Jaeger HM (2005) Phys Rev B 71:205412
30. Houbertz R, Feigenspan T, Mielke F, Memmert U, Hartmann U, Simon U, Schön G, Schmid G (1994) Europhys Lett 28:641
31. Taleb A, Silly F, Gusev AO, Charra F, Pileni M (2000) Adv Mater 12:633
32. Ohgi T, Sheng H, Nejoh H (1998) Appl Surf Sci 130:919